Chemical contrast in STM imaging of transition metal aluminides

T. Duguet [a,*], P.A. Thiel [b,c,d]

[a] CIRIMAT – Université de Toulouse, and CNRS, 4 allée Emile Monso, BP44362, 31430 Toulouse Cedex 4, France
[b] Ames Laboratory – US Department of Energy, Iowa State University, Ames, IA 50011, USA
[c] Department of Chemistry, Iowa State University, Ames, IA 50011, USA
[d] Department of Materials Sciences & Engineering, Iowa State University, Ames, IA 50011, USA

Keywords:
Scanning tunneling microscopy
Chemical contrast
Aluminium transition metal alloys
Valence band structure

A B S T R A C T

The present manuscript reviews recent scanning tunnelling microscopy (STM) studies of transition metal (TM) aluminide surfaces. It provides a general perspective on the contrast between Al atoms and TM atoms in STM imaging. A general trend is the much stronger bias dependence of TM atoms, or TM-rich regions of the surface. This dependence can be attenuated by the local chemical arrangements and environments. Al atoms can show a stronger bias dependence when their chemical environment, such as their immediate subsurface, is populated with TM. All this is well explained in light of combined results of STM and both theoretical and experimental electronic and crystallographic structure determinations. Since STM probes the Fermi surface, the electronic structure in the vicinity of the Fermi level (E_F) is essential for understanding contrast and bias dependence. Hence, partial density of states provides information about the TM *d* band position and width, *s*–*p*–*d* hybridization or interactions, or charge transfer between constituent elements. In addition, recent developments in STM image simulations are very interesting for elucidating chemical contrast at Al–TM alloy surfaces, and allow direct atomic identification, when the surface does not show too much disorder. Overall, we show that chemically-specific imaging is often possible at these surfaces.

* Corresponding author. Tel.: +33 5 3432 3439; fax: +33 5 3432 3499.
E-mail address: tduguet@ensiacet.fr (T. Duguet).

http://dx.doi.org/10.1016/j.progsurf.2012.05.002

Contents

1. Introduction

Transition metal (TM) aluminides are the subject of both basic and applied research, because they exhibit certain attractive properties [1,2]. These properties include good strength and stiffness at elevated temperature, plus low density. Nickel aluminides, for instance, are less dense than steel. TM aluminides – notably Al–Ni–Co alloys – are also widely marketed as permanent magnets [3], and exhibit promising shape-memory properties [4]. Surface properties of TM aluminides have received much attention, in part because these materials usually exhibit excellent oxidation and corrosion resistance. Some TM aluminides are quasicrystals, and exhibit properties associated with quasiperiodic structure, including surface properties such as low friction [5]. Refs. [6–21] provide a few examples of the many surface science investigations of TM aluminides.

The aim of the present review is to collect STM results obtained on TM aluminides, and to delineate trends in the ways that Al atoms can be distinguished from TM atoms in STM imaging. Being able to identify or differentiate elements on alloy surfaces is essential to the determination of adsorption sites and their chemical environment, including active sites for catalysis. This ability is equally important in quantification of surface segregation, comparison of surface vs. bulk structure, contamination level determination, nanostructuring, and other phenomena.

Basic structural information about surfaces can be used to engineer tailored surfaces. As an example, basic research has revealed that γ-Al_4Cu_9 grows epitaxially as a surface alloy on both Cu(1 1 1) and the fivefold surface of the icosaedral (i-) quasicrystal i-Al–Cu–Fe [22,23]. In the real world, this knowledge has been used to grow a γ-Al_4Cu_9 interlayer by magnetron sputtering, in order to solve the problem of poor adhesion between a quasicrystal and a metal [24]. To provide the basic surface information, STM is commonly used, along with spectroscopies and diffraction techniques. However, this might not be enough for a complete chemical description of the surface structure. It is usually a combination of surface sensitive techniques that allows scientists to draw conclusions about surface structures.

In this article, we will not describe atomic force microscopy studies, although some recent work shows its capability to identify elements on an atom by atom basis [25]. Under some circumstances STM can also reproduce those results [26–32], for instance with the use of inelastic tunneling [29]. We will also ignore surface state mediated phenomena, such as indirect interactions between adsorbates for which a comprehensive review has been published by Ternes et al. [33], or such as the manipulation of adatoms to create quantum corrals [34], for instance. Here, we focus on more typical STM experiments, where constant-current mapping, scanning tunneling spectroscopy (STS), and bias variation are commonly employed.

Since tunneling microscopy is sensitive to the Fermi surface, it is of great value to analyze STM data with the assistance of data from valence band probing techniques, and also electronic density of states (DOS) calculations. Some diffraction techniques can also be used for a complete surface structure determination, such as intensity profile analysis in low-energy electron diffraction (LEED I(V)), surface X-ray diffraction, or ion scattering, although in many cases they require some kind of *a priori* model.

STM is mostly sensitive to the local electronic density in the vicinity of the Fermi level (E_F). This is due to the fast decay with increasing energy difference from E_F, of the transition probability of

electrons from electronic states of the metallic tip, to electronic states of the sample. Therefore, when the valence band structure of an alloy is known, and can be deconvoluted with the aid of information about the surface partial DOS from calculations, one can interpret which element is giving the main contribution at E_F – therefore to the STM image contrast. Additionally, it is not very time consuming – in terms of computations – to simulate STM images once the surface DOS has been calculated. Overall, the analysis can lead to strong or weak conclusions depending on both the surface and the model. If one starts from a bulk-terminated model, the comparison with the real surface can be affected by defects, chemical segregation, relaxation, reconstruction, buckling, or rumpling. The modeling itself may be incapable of reproducing a bulk termination, because of an excessive number of atoms per unit cell, which would lead to non-convergence or non-realistic computing time. Finally, there are examples where viewing the STM contrast as resulting from the electronic density contour is not valid, because of adhesive tip–surface interactions, or local variation of the tip-surface distance (edge effect) [35–37].

Most of the STM studies presented below were conducted within the framework of the complex metallic alloys community (see for instance [38]). This community has devoted great effort to explaining surface formation and stabilization, adsorption, and properties, using combined work by experimentalists and theorists. Since complex metallic alloys are mostly Al-rich TM alloys, this provides an interesting pool of data for the broader audience of surface scientists dealing with surface aluminides and aluminide surfaces. Quasicrystals can be considered to represent an extreme point in the spectrum of complex metallic alloys, because their unit cell is so large that it is (ideally) infinite. Quasicrystals are atomically-well-ordered, but not periodic. Many of the studies presented in this paper involve quasicrystals, of two specific structural types: Icosahedral and decagonal. These can be considered as quasicrystalline in three and two dimensions, respectively. The decagonal phases are aperiodic planes of atoms that are stacked periodically (along the 10-fold axis), while the icosahedral phases have no periodic axis whatsoever. While many quasicrystals contain 60–70 atomic% Al—and these are obviously the only type considered in this article—the quasicrystalline atomic structure also occurs in many phases that do not contain Al at all.

The following section provides a general rationale for the ability to differentiate Al and TM atoms in STM, either from raw topographic images or from differences in bias dependence. Section 3 provides examples where the differentiation between Al and TM atoms is very clear, despite the fact that the structural arrangement is very complex. Section 4 highlights examples where DFT simulations have led to atomic identification on TM-aluminide surfaces. In the final section, the observations are generalized and summarized.

2. Electronic structure

The most widely-used theory for explaining STM images of metallic surfaces is the theory developed by Tersoff and Hamann [39], which built upon Bardeen's theory for the tunneling current in a metal–insulator–metal junction [40]. In the Tersoff–Hamann model, the symmetry of the tip wave function is considered spherical, and the surface wave function is developed on a plane wave basis. With these characteristics, the tunneling current can be expressed as:

$$I \propto (eV - E_F)\frac{eh^3}{m^2}\rho_{\text{tip}}(E_F)\rho_{\text{sample}}(eV - E_F) \tag{1}$$

where $\rho_{\text{tip}}(E_F)$ is the electronic DOS of the tip at the Fermi level, and $\rho_{\text{sample}}(eV - E_F)$ is the electronic DOS of the surface at energy eV. e is the electron charge, h is Planck's constant, and m is the effective mass of the electron.

Since bias voltages $(eV - E_F)$ used in STM are small, expression (1) shows that the tunneling current is mostly sensitive to the local electronic density in the near vicinity of E_F. Therefore, there is a strong dependence on the details of the valence band structure of the surface under consideration. Sometimes – as in the case for the STM investigation of the Ni_3Al surfaces described in Section 4 – a more complex origin has been proposed for the STM contrast. However, with most Al–TM surfaces, it is

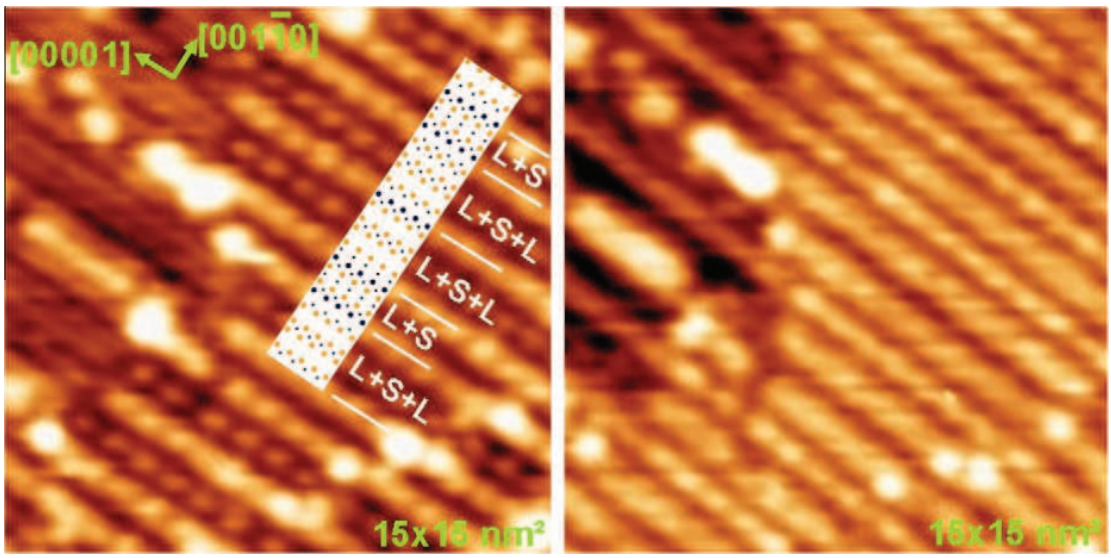

Fig. 1. STM images of a TM-rich terrace on twofold d-Al–Cu–Co, at two opposite biases. Left: (−1.2 V, 0.5 nA), Right: (+1.2 V, 0.5 nA). Dark (blue) dots represent Al atoms. Bright (orange) dots represent transition metal atoms. Dot size is a function of their vertical position. Reproduced from Ref. [41]. Copyright 2009 by the American Physical Society. (For interpretation of the references to colour in this figure legend, the reader is referred to the web version of this article.)

always important to analyze the electronic structure of the given surface, and if possible to simulate the STM images.

Experimentally, when the tip is biased negative or positive relative to the sample, the filled or empty states of the sample are probed and mapped. In this article, negative bias voltages will consistently correspond to filled-states images, and vice versa. The consequence of changing bias polarity is that the STM image switches between filled states and unfilled states. The bias (polarity) dependence of the STM image thus depends upon the asymmetry in the DOS on either side of E_F.

Some contrast between Al and TM atoms in a typical STM image is therefore expected if these two types of atoms contribute differently to the density of states at E_F. Following are the main features that should be considered when analyzing STM data of TM aluminides, along with their electronic DOS. Examples are developed in the following sections.

(i) Which element(s), and which state(s) of this element(s) dominate(s) the DOS around E_F? If the surface density of states at E_F is dominated by Al *s*- and *p*-like states, and the TM *d*-like states lie deeper in the valence band, then Al atoms are imaged as topographic protrusions, relative to the TM atoms. This situation is often observed. However, if a TM *d*-like band is present in the vicinity of E_F, it will overcome the other states' contributions and likely create an obvious bias dependence.

(ii) Is there any *s*–*p*–*d* hybridization between Al and TM atoms? In some cases, Al *sp*-like states hybridize with TM states, leading to little contrast in a normal STM image. Actually, hybridized states can have concomitant density variations, and therefore similar values.

(iii) What kind of bonding exists in the alloy? Complex metallic Al–TM alloys, for instance, are composed of highly coordinated clusters, where a covalent character has often been predicted, and/or observed, within the cluster. Then, a build-up of electronic density can occur between some atoms, leading to STM contrast between atomic sites. Additionally, if bonding–antibonding orbitals are asymmetric, and close to E_F, then bias dependence is expected.

(iv) Finally, the TM valence band exhibits a higher asymmetry than the Al one, thus leading to a larger change in contrast with changing bias for TM atoms, than for Al atoms. As we shall see, this provides an especially useful and obvious way for distinguishing between the two types of metal atoms.

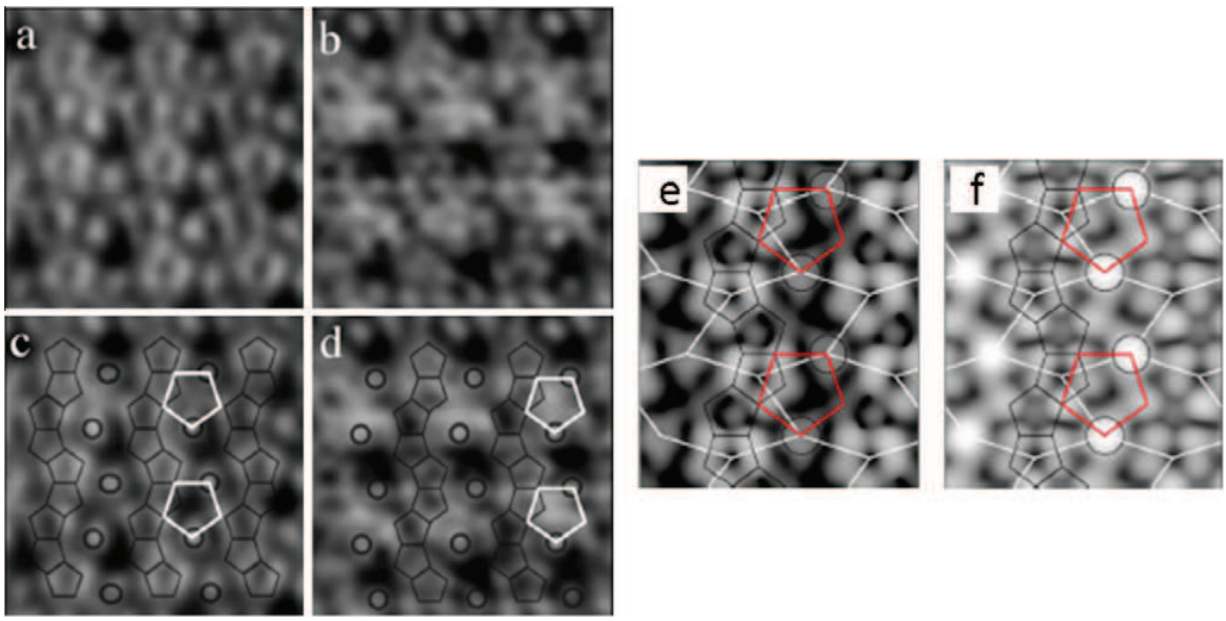

Fig. 2. STM images of the T-Al(Mn,Pd)(010) surface imaged at $V_{bias} = -0.4$ V and $I_t = 0.36$ nA (a), and another region imaged at $V_{bias} = 0.6$ V and $I_t = 0.50$ nA (b). (c and d) Show the same images with the relevant model tiling. (e and f) Are the simulated STM images at −0.4 and +0.4 V voltage biases, respectively. Reproduced from Ref. [57]. Copyright 2010 by the American Physical Society.

3. Simple chemical identification in rather complex systems

There have been some systems where bulk structural models, diffraction, or DFT calculations, combined with STM experiments, rendered possible the elemental identification of surface atoms. Surprisingly, one of the simplest systems to begin with has a high degree of structural complexity: the twofold surface of the decagonal (d-)Al–Cu–Co quasicrystal [41]. Decagonal structures are schematically represented by a pentagonal prism that requires five indexing vectors: they define four aperiodic twofold axes in the pentagonal basis and one periodic 10-fold axis, orthogonally. Therefore, a twofold surface contains two high-density crystallographic axes that are perpendicular. One is periodic whereas the other is aperiodic. Periodicity (or aperiodicity) does not matter for the purpose of this paper but it explains the atomic arrangement shown in Fig. 1, where atomic rows run along the periodic direction, labeled [00001].

The structural analysis of this surface was conducted by starting with a bulk model [42,43], in which three families of dense atomic layers were identified as likely candidates for surface terminations. These three terminations were also found at the surface, in the form of the three observed terrace types. One type was pure Al, whereas the other two contained transition metal atoms (15% and 40–50%, respectively). The one containing 40–50% of TM metal will be referred to as the TM-rich terrace. Fig. 1 shows a region that is predominantly a TM-rich terrace, at positive and negative biases. Rows whose contrast does not change much with bias are identified as mixed Al–TM lines, whereas other rows are made of TM metal atoms only, based on the overlaid model (where bright (dark) dots correspond to TM atoms (Al atoms)). The bias dependence of transition metals comes from localized *d*-like states of Co in the unoccupied band, as determined by DFT calculations of the electronic density of states of the relevant structural model [44]. d-Al–Ni–Co is isostructural to the d-Al–Cu–Co quasicrystal. Its twofold surface has also been investigated with STM, and bias dependence is similarly observed. Fig. 3 of Ref. [45] shows two STM images at two opposite biases. A well-defined subset of atomic rows shows a strong bias dependence, whereas other subsets' bias dependence is milder. Analysis is based on a structural model implying that the surface atomic layer is pure Al. Thus, contrast is explained by the influence of subsurface TM atoms lying 2 Å underneath the most bias-dependent atomic rows at the surface. Consequently, the surface is most likely pure Al, but the chemical environments of the different Al rows influence drastically their local electronic contour, as seen in STM

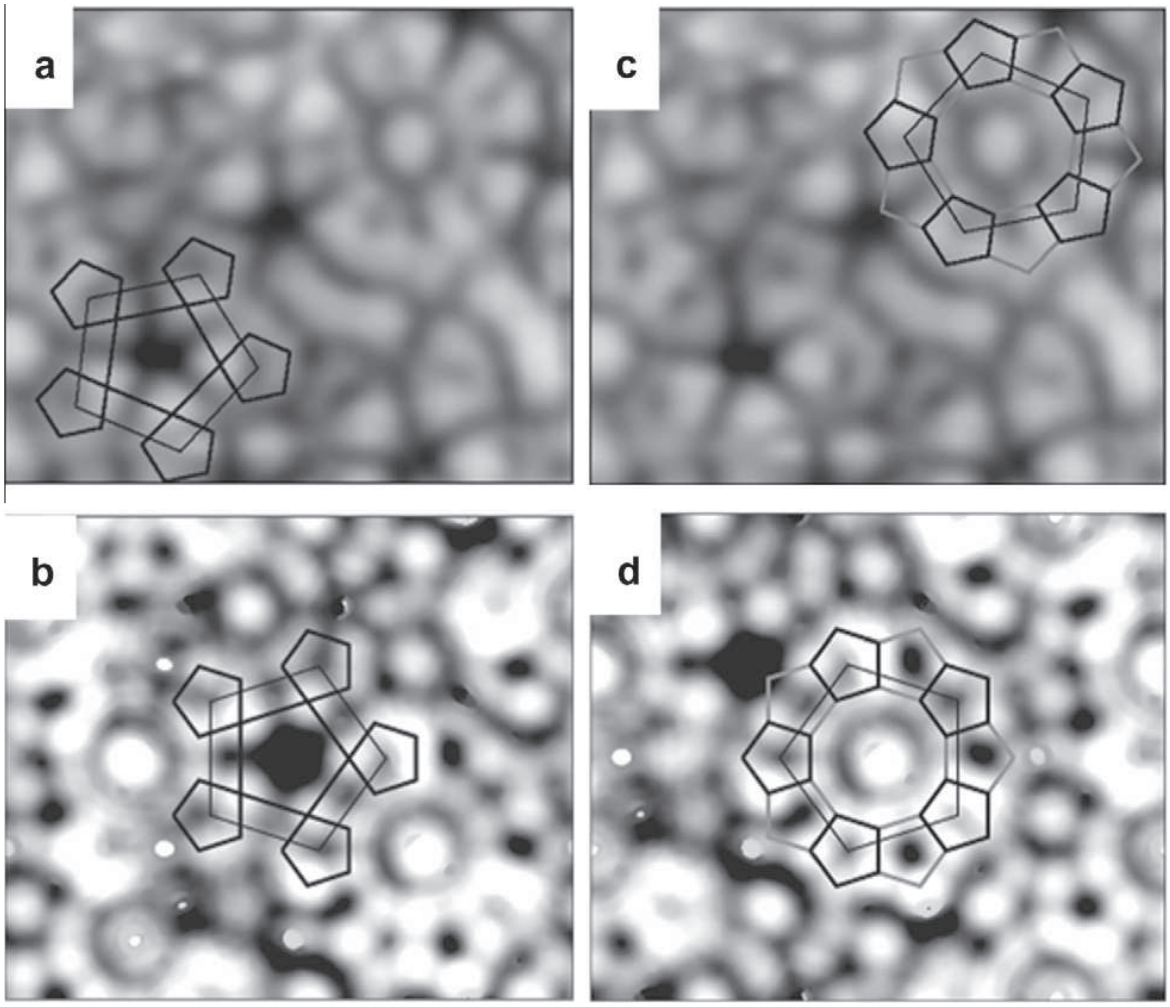

Fig. 3. (a and b) Comparison of experimental (top) and calculated (bottom) STM images of the dark pentagonal hole: the dark star DS. The area of the images is 39.5 × 32.9 Å. The DS is formed by a surface vacancy surrounded by a pentagon of Al atoms separated by 4.79 Å and a pentagon of Pd atoms of the same size forming in the STM image dark "arms" of the DS. (c and d) Same layout for the STM images of the white flower WF. The area of the STM image 39.5 × 32.9 Å is the same as the size of the structural model. Reproduced from Ref. [59]. Copyright 2006 by the American Physical Society.

imaging. Recently, it was shown by STS on the other (inequivalent) twofold surface of d-Al–Ni–Co, that the local electronic density of a certain subset of rows, which we define as subset A, could be 30% higher than the other rows (subset B) at negative bias (occupied states) [46]. This is due to the different asymmetries of the differential conductances (dI/dV) of the two subsets of rows, on each side of the Fermi level. This leads to a relatively higher bias dependence for subset A, as similarly mentioned in the previous paragraph for the Al–Cu–Co system. Interestingly, the surface structure determination by high-resolution STM indicates that the rows that are not strongly bias dependent are pure Al [47].

Finally, the reason why twofold decagonal surfaces are very suitable for chemical identification of elements comes from their atomic row arrangements, leading to a 1-dimensional or line-by-line bias dependence. One can see, in the overlaid model layers in Fig. 1, that periodic lines of like-atoms are stacked in the [0 0 1–1 0] direction. In terms of imaging and bias dependence of STM contrast, the analysis is easier than for a more conventional surface, where each individual atom of the unit cell potentially shows different two-dimensional in-plane coordination. The latter results in a more complex electronic density contour, hence a less straightforward STM contrast analysis.

The 10-fold surface of d-Al–Ni–Co has also been studied, but no clear conclusions can be given because two articles published at about the same time are contradictory [48,49]. Combined ion scattering spectroscopy (ISS), Auger electron spectroscopy (AES), and STM showed that the 10-fold surface of d-Al–Ni–Co may be strongly enriched by Al, with a ratio of Al atoms to TM atoms equal to 8:1 (As a

reference, the bulk composition corresponds to a ratio of 2.6:1). The areal density of protrusions imaged by STM was the same as the density of Al atoms determined from ISS, leading to the assignment of the protrusions as Al atoms. The authors concluded that the surface underwent significant Al surface segregation to produce a nearly pure Al termination, and their model agrees well with the experimental image [49]. However, this is in contradiction with the LEED I(V) and STM study of another Al–Ni–Co sample of similar bulk composition [48], where the top plane deduced from LEED corresponds to a bulk truncation composed mainly of TM atoms. Additionally, the match between the LEED model and the experimental STM image is excellent. Which of these two reports is correct could probably be determined from measurements of the bias dependence or from STS experiments, since little bias dependence is expected for a pure Al termination. To our knowledge, there is no measurement of bias dependence on this surface.

4. Chemical identification supported by simulated STM images

Al–TM alloy surfaces have also been investigated along with *ab initio* calculations, with the aim of simulating STM images. For this purpose, the supercell method is used, where a unit cell consists of a slab of the atomic structure with a vacuum space above. The DOS is calculated at the surface that is virtually created at the interface between vacuum and the atomic layers. Then, the Tersoff–Haman model constitutes a reasonable approximation for simulating STM images, where the electron density map is constructed from the center of a spherical tip, fixed at a certain distance from that surface, into the vacuum space [39].

Deniozou et al. recently used STM, DFT calculations and photoemission to study the (0 1 0) surface of the Taylor (T-) phase Al_3(Pd,Mn) [50,51]. T-Al_3(Pd,Mn) phase is a ternary solid solution of Pd in the binary orthorhombic T-Al_3Mn with interesting magnetic [52–55] and mechanical properties [56], for instance. Their results indicate that the surface is not a perfect bulk truncation but retains the main features of the bulk model termination [57]. Surface defects exist, consisting of atom vacancies and some chemical disorder.

The overlaid model (see Fig. 2c and d) is described as zig–zag chains of mixed Al-TM pentagons (small black pentagons) alternating with zig–zag Mn atomic lines (open circles). The zig–zag chains of pentagons are not strongly bias dependent. This is also predicted from the simulated images of Fig. 2e and f. In between the chains, bias dependence is complex, at least experimentally, since disorder is present, as mentioned above. However, in terms of chemical composition, the regions between chains are mainly occupied by Mn atoms, based on the model. The authors assert that the Mn *d*-band is most likely responsible for the electronic structure in the vicinity of the Fermi level [57]. Thus, we assign the bias dependence of the regions between pentagonal chains as resulting from this partial contribution of Mn to the DOS. As a side remark, we would like to point out the similarity of this surface with the TM-rich terraces of d-Al–Cu–Co, shown in Fig. 1. Actually, mixed Al–TM rows or chains alternate with pure TM rows or chains, for the d-Al–Cu–Co and T-Al_3(Mn,Pd) phases, respectively. In both cases this leads to a row-by-row bias dependence, i.e. bias dependence is only observed in the direction perpendicular to the rows.

Another feature of the T-Al_3(Mn,Pd) surface is the presence of ‘‘dark star’’ motifs. They can be seen at positive bias, in Fig. 2b, for instance. Dark stars, along with ‘‘white flowers’’ are probably the most discussed and studied motifs in STM imaging of icosahedral (i-) quasicrystals. They decorate the icosahedral fivefold surfaces, and are known to result from the truncation of Mackay and Bergmann clusters that, in turn, decorate the bulk structure [58]. Fig. 3 shows the dark stars and white flowers observed experimentally (a and c) on the fivefold surface of the i-Al–Pd–Mn quasicrystal [59]. Simulated STM images are also shown below (b and d). The dark star is formed by a central vacancy surrounded by an Al pentagon and a Pd pentagon of the same size, but rotated by $\pi/10$. The Al pentagon appears bright in the STM image, whereas the Pd pentagon forms the dark arms of the dark star. As shown for the bulk i-Al–Pd–Mn system using soft X-ray spectroscopies – which allow determination of the partial electronic densities of the constituent material in the valence band (soft X-ray emission spectroscopy), and in the conduction band (soft X-ray absorption spectroscopy) – the Fermi energy is mainly populated by Mn and Al states, whereas Pd states are further away from E_F [60]. This could explain why Pd is not imaged by STM in this system.

Fig. 3c and d show the white flower motif. It is formed by a central Mn atom, surrounded by 10 Al pentagons. Sometimes, unlike in Fig. 3, the Al pentagons are not atomically resolved and appear as single bright spots forming the leaves of the white flower. Again, Al and Mn atoms are bright in the STM image, most likely because of their electronic contributions to the Fermi surface, as opposed to Pd states that are located further into the center of the valence band. To the authors' knowledge, neither dark stars nor white flowers were reported as being bias dependent in STM imaging of i-Al–Pd–Mn, nor was it the case in the i-Al–Cu–Fe system. This can be explained, for Al–Pd–Mn, from the partial electronic densities of Al, Mn, and Pd, as measured by soft X-ray spectroscopies on an i-Al–Pd–Mn quasicrystal, and shown in Fig. 1 (valence band) and 2 (conduction band) of Ref. [60]. Al interacts strongly with Mn, as shown by the coincidence of the Mn *3d* maximum, with the Al *3p* shoulder in the valence band, near E_F. The same behaviour is observed in the conduction band. Therefore, the absence of bias dependence of Al and Mn atoms on the surface may be due to a strong interaction of Mn and Al, resulting in small variation in the electronic DOS in the vicinity of E_F.

The (1 0 0) surface of orthorhombic (o-)$Al_{13}Co_4$ has been studied by a similar method [61]. But in that case, the surface exhibits partial desorption of some less strongly bonded atoms. This is likely due to the presence of a different bonding character (more covalent) inside bi-pyramidal motifs that decorate the surface. The atomic arrangement is shown in Fig. 4a, along with an experimental STM image (b), and simulated images (c–f). Different terminations were initially tested for simulating the STM images, without apparent success. The authors mainly pointed out the lack of contrast and bias dependence of the atoms at the center of the Al pentagons (so called Co(+) and Co(−) atoms) [61]. Recently, LEED I(V) experiments [62], combined with DFT calculations [63], resulted in a thorough structure determination. The (1 0 0) surface of o-$Al_{13}Co_4$ corresponds to a truncation of the bulk structure at specific positions between flat and puckered atomic layers, exhibiting low-density terminations with missing atoms for which desorption energies are relatively low. A moderate annealing temperature is sufficient for such desorption. Surface features are the very stable bi-pyramidal motifs of composition $Al_{10}Co_2$, stabilized by strong Co–Al–Co bonds, and connected by so-called glue atoms

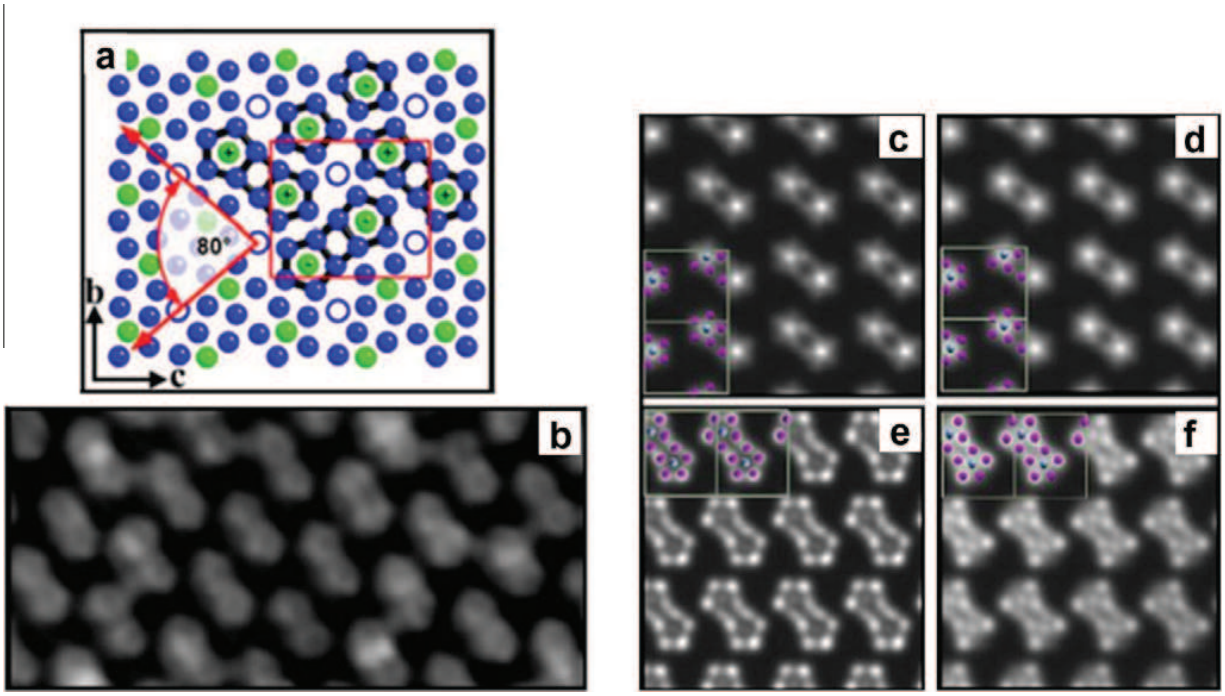

Fig. 4. (a) Puckered atomic layer P2, extracted for a bulk model. Co is represented in bright contrast (green) and Al as dark (blue). Depending on the height of the Co atoms [(+) or (−)] within the puckered planes, two sets of bi-pentagonal motifs are present. (b) Experimental 5 × 10 nm^2 STM image recorded with $V_{bias} = -1.3$ V and $I_t = 0.08$ nA. (c and d) Respectively unrelaxed and relaxed simulated STM images (5 × 5 nm^2, $V_{bias} = -1.3$ V) of the P^+ model termination with the Co(+) subset of motifs only. (e and f) Idem with the Co(−) subset of motifs. Reproduced from Ref. [61]. Copyright 2009 by the American Physical Society. (For interpretation of the references to colour in this figure legend, the reader is referred to the web version of this article.)

of Al. Sometimes, missing Co atoms at the center of bi-pyramidal motifs are responsible for the non-bias dependence, and for the lack of contrast in the experimental STM images. This is helpful in the picture we are drawing about the contribution of TM atoms *vs.* Al atoms in STM contrast and bias dependency.

Interpretation resulting from the comparison between experiments and calculations in this system is not straightforward because surface preparation at elevated temperatures in UHV is responsible for the partial desorption of surface atoms, whereas STM is conducted at room temperature. This leads to a deviation from the ideal model determined by *ab initio* calculations.

Surprisingly, the interpretation is much simpler for the monoclinic (m-) (001) surface of Al_9Co_2. m-Al_9Co_2 is also considered to be a complex metallic alloy, but with a rather simpler structure than the o-$Al_{13}Co_4$ phase. In that sense, it shares some similar features like strongly bonded Al–TM clusters with covalent character. A complete surface study of the (001) surface has been conducted by ultra-violet and X-ray photoelectron spectroscopies, STM, STS, LEED, and DFT calculations of local and total DOS, leading to STM simulations. It is concluded that the surface corresponds to a bulk truncation at a pure Al termination, with no segregation of Co, and no desorption of surface atoms. Those results hold for different surface preparation temperatures in UHV [64].

Despite the absence of TM atoms at the surface of m-Al_9Co_2, there exists a slight bias dependence of the STM contrast. Fig. 5 shows an experimental STM image of the (001) surface, where bias has been reversed at the white horizontal line. STM simulations of the pure Al termination corroborate this observation, and show that bias dependence is located in between Al atoms, while contrast et al. atom sites remains constant (see P_{Al} simulations in Fig. 8 of Ref. [64]). We tentatively explain this bias dependence by both the build up of electron density between Al atoms in the covalent bonding, and by an asymmetry between the two frontier orbitals.

Actually, one has to be careful with STM contrast since it can or cannot reflect the underlying atomic structure. Additionally, sometimes, local density of states and electronic states localization is insufficient for explaining STM contrast. For example, NiAl(110) is known to exhibit a stoichiometric surface composition, with Al atoms buckling outward by 0.22 Å [65]. The only species seen as

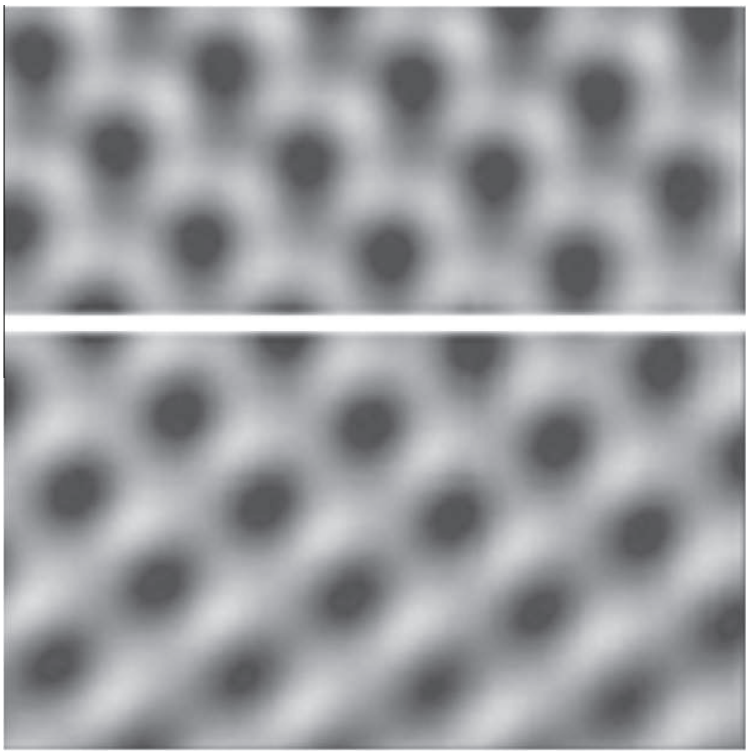

Fig. 5. 4×4 nm Fourier filtered STM image (tunneling current = 0.36 nA). The horizontal white line indicates a bias change from −1.3 V (above) to +1.3 V (bottom) while scanning. Reproduced from Ref. [64]. Copyright 2011 by the American Chemical Society.

protrusions in STM are the Al atoms [66]. A similar effect holds true for Ni_3Al (001) and (111) surfaces, where a (2×2) reconstruction apparently occurs. Thus both Al and Ni atoms are *effectively* present at the surface, but Ni atoms remain invisible. Jurczyszyn et al. studied both surfaces with the combination of STM and calculations, with a sample bias of +20 mV, i.e. tunneling into the sample unoccupied states [35]. Their calculation formalism implies that tunneling corresponds to the superposition of individual tunneling processes through different channels (orbitals) of the tip and the sample. This also allows analysing those individual channels in order to determine their individual and/or combined role in the final tunneling process. It appears that Al and Ni p_z and s orbital interferences are mainly responsible for the experimental STM contrast. For simulating STM images, the topmost part of the tip was represented by a pyramidal cluster of W atoms, and scanning was simulated in constant height mode. Ni_3Al(111) and (001) STM images were successfully reproduced. We now detail their explanation of the STM contrast, based on the surface electronic properties described in Ref. [35], and stressed in Fig. 6.

Fig. 6a and b show the partial contributions of the Ni and Al s and p_z states to the DOS, for the Ni_3Al(001) and Ni_3Al(111) surfaces, respectively. d states were neglected, because they contribute only a few percent to the tunneling current. The absence of contrast of Ni atoms in STM imaging could have been explained by a difference in the DOS at E_F between Ni and Al. Such a difference is visible on Ni_3Al(111) in Fig. 6b, where the DOS of Al p_z states is 20% higher that that of Ni. But, since Al and Ni states contribute equally to the Ni_3Al(001) surface DOS (a), this difference cannot account for the lack of Ni contrast on both surfaces. The difference actually lies in the intra-atomic interactions of the s and p_z states, for Al and Ni atoms, respectively. Fig. 6 c and d show that the total conductance is dominated by Al states when intra-atomic interactions are taken into account (c), whereas both Al and Ni states would contribute if these interactions were neglected (d). The authors explain this effect by the relative energy of the states that are active in the tunneling process versus the potential energy of the s

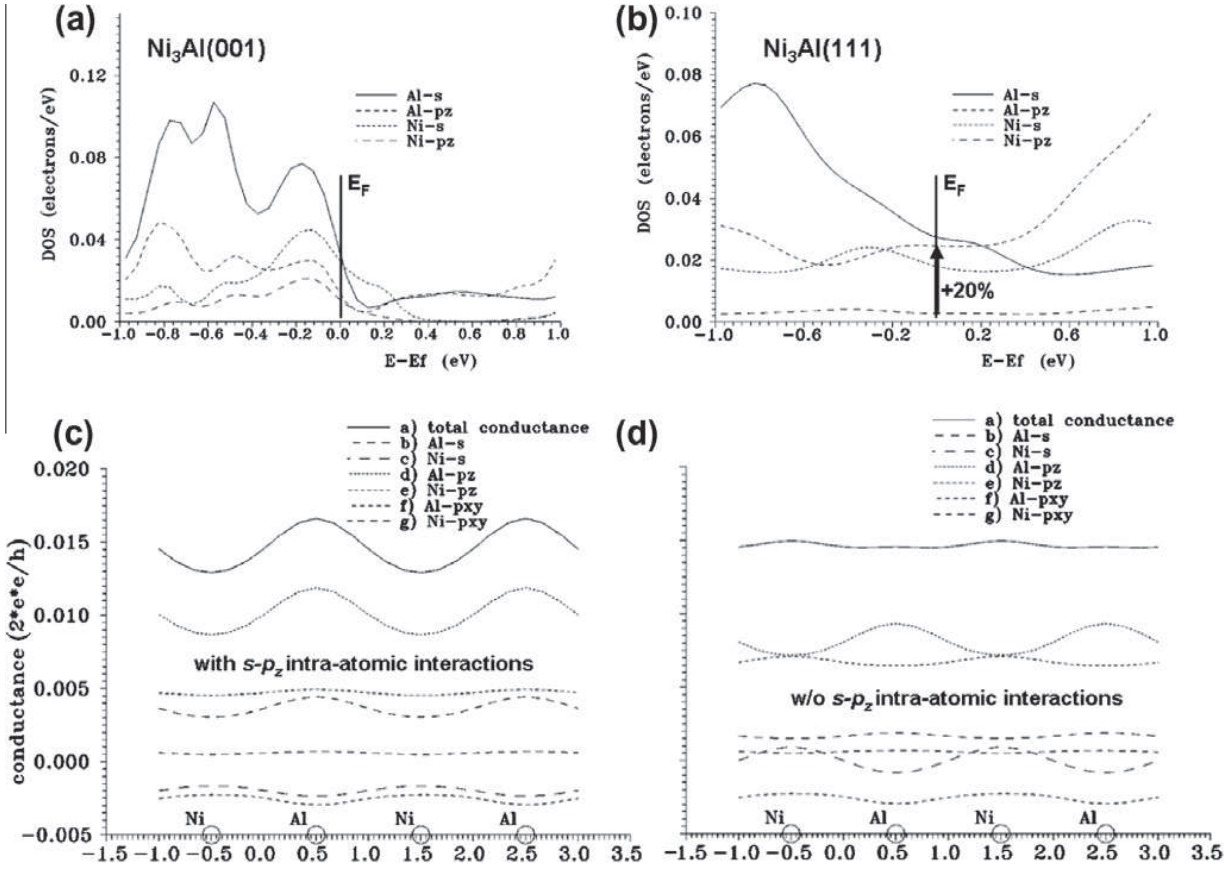

Fig. 6. (a and b) s and p_z DOS of surface atoms on Ni_3Al(001) and Ni_3Al(111). (c and d) Total and partial conductances calculated with and without taking into account s–p_z intra-atomic interactions in the model. Reproduced from Ref. [35]. Copyright 2003 by the American Physical Society.

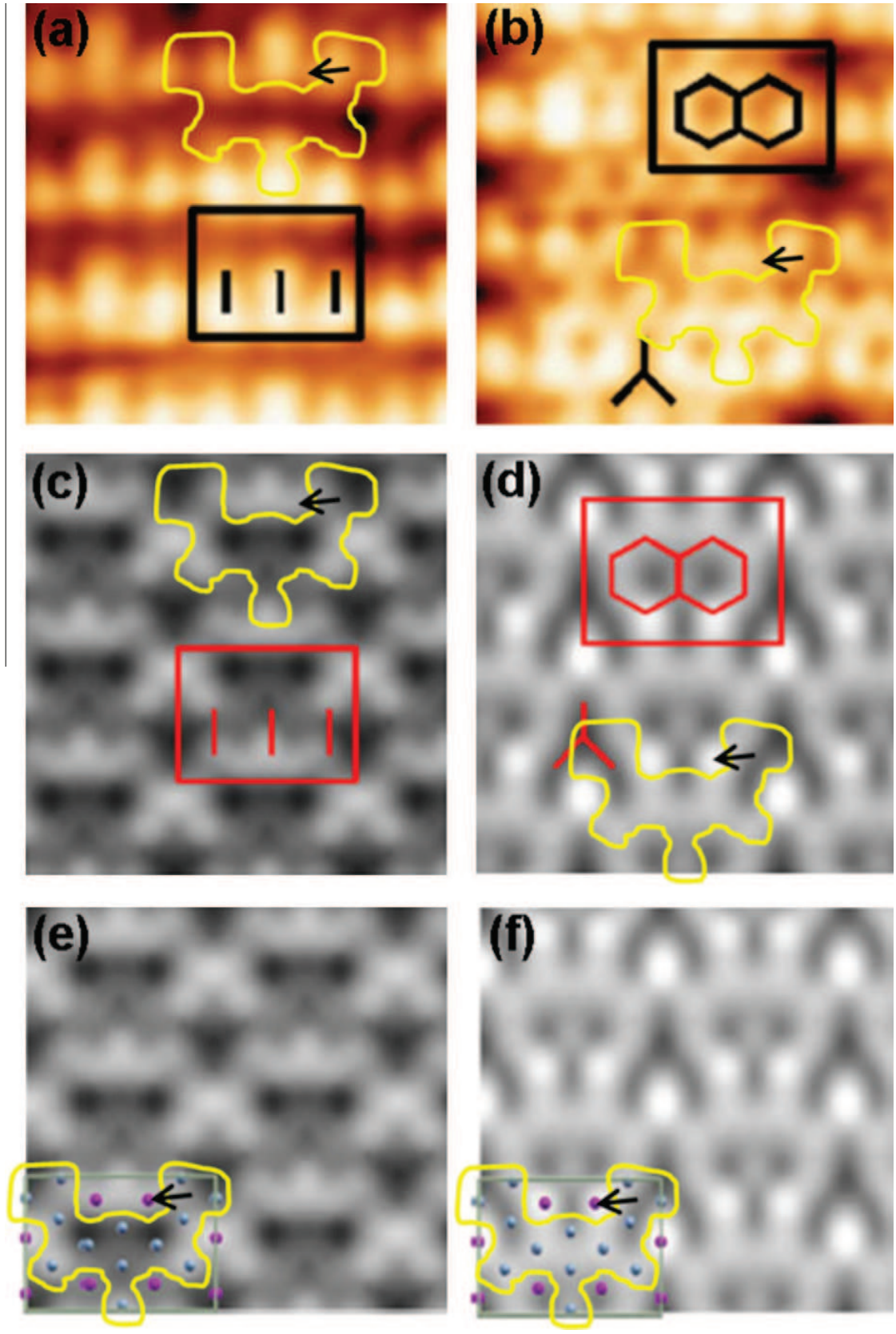

Fig. 7. (a and b) Experimental STM images of a PF termination. (c–f) Corresponding simulated images. Left column: −0.5 V. Right column: +0.5 V bias voltages. The model unit cell is represented in (e and f) with Al as dark (purple) and Cu as bright (blue) circles. See text for details about schematics. Reproduced from Ref. [70]. Copyright 2010 by the American Physical Society. (For interpretation of the references to colour in this figure legend, the reader is referred to the web version of this article.)

and p_z orbitals. When tunneling occurs through significantly lower energies, the intra-atomic s–p_z interaction lowers the current through s and p_z states. Inversely, when the tunneling energy is between s and p_z energies the s–p_z interaction increases the tunneling current. In STM, tunneling occurs in the vicinity of the Fermi level, which is well below the energies of the Ni s and p_z orbitals, but in between Al s and p_z orbitals energies in Ni_3Al. Therefore, current tunneling through Al is higher, whereas current tunneling through Ni is lower. The overall effect is the exclusive contrast of Al in STM imaging of Ni_3Al. The effect is less pronounced in the $Ni_3Al(1\,1\,1)$ surface than in the $(0\,0\,1)$ surface, because the former surface is denser, and hence interatomic interactions are stronger. It is finally worth mentioning that $Ni_3Al(1\,1\,1)$ and $(0\,1\,1)$ electronic and structural properties have also been studied in the framework of the density functional theory, with the supercell method. A good agreement has been found between LEED I(V) and a relaxed bulk model, and also between STS spectra and calculated local DOS [67].

On the other hand, $Fe_3Al(1\,1\,1)$ illustrates a case where the surface is indeed pure Al. Below a critical temperature T_c, it shows a pure Al $(\sqrt{3} \times \sqrt{3})$R30 reconstruction, on top of Al-enriched Al–Fe layers. Above T_c, a phase transition is accompanied by the occurrence of Fe-rich terraces [68].

γ-$Al_4Cu_9(1\,1\,0)$ has also been studied by means of STM, LEED and *ab initio* simulations, both as a surface alloy [22,23,69] and as an alloy surface [70]. As a surface alloy, it was formed by mild annealing of thick (above 10 monolayers, typically) Cu films deposited under UHV conditions, on fivefold i-Al–Pd–Mn [69] and i-Al–Cu–Fe [23]. In these cases, five rotational domains were clearly identified by LEED and STM as being the $Al_4Cu_9(1\,1\,0)$ phase. Then, similar observations were made by growing Al_4Cu_9 as a surface alloy in the $Cu(1\,1\,1)$/Al system [22]. There, DFT simulations showed a good match with the experimental STM images, but also pointed out the presence of defects. Finally, the alloy surface was studied using a large single-grain of the Al_4Cu_9 phase cut to expose the $(1\,1\,0)$ surface [70]. The surface exhibits three types of terminations (two puckered and one flat), with varying surface areal coverage, depending on thermal treatment. However, the most stable terminations were found to be the puckered ones, both experimentally and theoretically. Since they contain two more Al atoms than the flat termination, they are richer in the element of lower surface energy (Al) *and* denser, and therefore, more stable. The comparison of their calculated surface energies confirmed this [70]. The experimental and simulated STM contrasts are very bias dependent for both puckered terminations. Fig. 7 shows one type of puckered termination (PF) at negative (left) and positive (right) biases.

This figure illustrates part of our general picture, which is that bias dependence is caused by TM atoms whereas Al atom contrast remains almost unchanged. To underline this, we modified the original figure by encircling a surface area covered by Cu atoms only in the model surface unit cell (see Fig. 7 a–e, yellow-bright line). The bias dependence of this region is obvious if one compares Fig. 7 a *vs.* b, and c *vs.* d. It is almost a contrast inversion in the simulations! Also, it is startling how good the match is between Fig. 7b and d in that region. Finally, an Al atom is followed and marked by the black arrow on all the images to point out its small contrast change with bias. Al atoms appear bright under both scanning conditions. The discrepancies between simulated and experimental images led the authors to the idea that the surface may be enriched by Al through surface segregation. An attempt has been made to simulate the STM contrast of pure Al terminations, though keeping the atomic arrangement of the bulk alloy model. A bad correspondence was obtained. Thus either the pure Al assumption is wrong, or the model used (Tersoff–Hamman [39]) is not suitable for a realistic simulation of this system. If it is pure Al, then STM imaging might be strongly influenced by adhesive tip–surface interactions [37], and scanning with a tungsten tip may induce favored tunneling through localized d-states that are ignored in the Tersoff–Hamman approximation, where the STM tip is assumed to have a spherical character only.

5. Conclusions, general trends and discussions beyond the Al–TM case

This review article aims to demonstrate how "usual" scanning tunneling microscopy can be used and how images can be analyzed in order to identify aluminum and transition metal atoms. This statement is based on the authors' own experience and on other contributions dealing with the surface characterization of transition metal aluminides. Chemical differentiation is possible by combining

STM experiments with different techniques, and also with theoretical calculations that reveal the electronic structure of the surfaces of interest. Actually, STM is sensitive to the electronic density contour of the surface, close to the Fermi level. Hence, a fairly good parallel can be done between an STM image and the electronic density, at defined scanning conditions (bias voltage and current). Sometimes, this simple picture is not valid because of complex phenomena occurring in the tunneling junction or within the material itself, such as in the NiAl system described in section 4. However, our assessment is relevant for most of the cases described in the literature.

We emphasize the fact that Al and TM atoms show a different contrast *and* response to bias variation. It is first based on the observation that bias dependent surface regions contain transition metal atoms, and that Al is not bias dependent, except when coordinated with transition metal atoms. This is related to the energy positions of their partial contributions to the total electronic density. If the TM *d*-like states lie deep in the valence band, then Al atoms represent the main contribution to the DOS, and they are imaged as topographic protrusions, relative to the TM atoms. If a TM *d*-like band is present in the vicinity of E_F, its spectral weight will overcome the other states and likely create an obvious bias dependence. A striking example can be found in Section 3, with the twofold decagonal Al–Cu–Co surface, where one side of the Fermi surface is populated with Al *sp*-like states and where Al atoms seem to buckle outward (Fig. 1, left), and where the other side of E_F exhibits a strong contribution of Co *d*-like states, giving rise to a dramatic change of contrast with the bias voltage (Fig. 1, right). Additionally, careful attention should be paid to *s*–*p*–*d* hybridization between Al and TM atoms. Electronic density differences in the valence band are less expected between two strongly hybridized elements; hence, differentiating Al from TM might be less straightforward due a limited chemical contrast. Also, if bonding partially shows a covalent character, as is observed in some complex metallic alloys, then electrons can be localized between atoms, giving rise to STM contrast where no atom is present. The shape of the frontier orbitals is also important in that case, since asymmetry could be responsible for the observation of a local bias dependence, where the electron density builds up.

We now consider chemical contrast with a larger perspective than only Al–TM surfaces. In a simplistic view, one could say that *sp*-like metals possess a relatively flat DOS in the vicinity of the Fermi level. Hence, no STM contrast variation would be expected for Al or free-electron like metals whereas it would occur for transition metals or lanthanides because of the localization and spectral weight of *d*– and *f*– bands. An example – apart from the Al–TM case – is the absence of STM imaging of the Sn atoms at the (0 0 1) surface of Pt_3Sn whereas the Sn atoms are visible with diffraction techniques [71]. In this latter system, the calculated local electron density at Pt atomic sites is much higher than at Sn, because of strong Pt *d*-like states centred at +0.9 eV.

Nevertheless, hybridization has to be taken into account. The *sp* metals eventually hybridize strongly with the other element(s), giving rise to a similar electronic density variation around E_F resulting in a poor STM contrast. Therefore, it is obvious that localized states such as *d*-like bands can generate more contrast for a given element, but it depends on the energy at which those states lie and on the level of hybridization. For example, there are systems, such as Al–Li–Cu or Al–Mg–Zn, which behave as pure *sp*-like metals because *d*-bands are forced deeper into the valence band and do not affect the valence electronic properties [72]. In these latter cases, though there is no experimental evidence for the absence of chemical contrast in STM, it would definitely not be attributed to *d*-bands.

Finally, chemical contrast also exists in STM imaging of TM-TM alloy surfaces. Schmid and Varga reviewed the STM studies that showed chemical contrast in these systems [73]. There are mainly three different cases. (i) PtNi(1 1 1) that does not exhibits chemical contrast because Pt and Ni local DOS are similar. There, the authors observed chemical contrast thanks to a favoured chemical interaction of the Ni atoms – rather than the noble Pt – with the tip that has been accidentally covered with some adsorbate (likely S or O contamination from the substrate) [74]. In the Pt–Rh system, there already exists little chemical contrast because of differences in the local DOS of Pt and Rh. Consequently, Pt shows a lower apparent height and appears darker. This contrast has been drastically enhanced by the functionalization of the STM tip [75]. The reverse contrast is observed in the Pt–Co system where Pt appears brighter. This surface was not investigated with a functionalized tip [76]. These three last examples illustrate the fact that STM contrast can originate from tip–surface interaction(s), electronic contour, or topography, or combinations thereof.

We can now tentatively propose some would-be-interesting STM experiments by considering electronic features of a few systems – providing that surface DOS and surface structure are not drastically different to that of the bulk. For instance, in the partial DOS calculations of the Mg–La phases, La *5d* and *4f* bands were found approx. 10 times more intense than Mg *3s*, *2p* [77]. Since La *5f* is at approx. +1 eV above the Fermi level, La would likely present a stronger contrast if unoccupied states were probed with STM. An interesting combination of the above examples would be the STM study of the "free electron-like-Rare Earth-TM" system $MgLa_4Co$. The Mg partial DOS is flat whereas Co *3d* and La *4f* are very intense *and* localized at -2 eV and +2–2.5 eV, respectively from E_F [78]. Therefore, we postulate that the three elements would be distinguished by varying the STM tip bias. A counter example is the decagonal Al–Ni–Co quasicrystal where Ni and Co bands overlap, and for which no contrast has been observed between the two.

To conclude, elemental identification in STM is extremely important in studies involving alloy surfaces, including studies of adsorption, diffusion, nucleation and growth, contamination, surface segregation, etc. However, elemental identification is never straightforward, and strongly relies on the availability of good structural models, plus complementary information. Our review has been limited to Al–TM systems, but we hope that it may provide a general framework for STM users who need to identify atomic features in experimental images, and that this framework will be extended to, and tested in, a greater number of alloy systems.

Acknowledgments

We would like to thank V. Fournée and J. Ledieu (CNRS, Nancy, France) for fruitful discussions. Work at the *Institut Jean Lamour* was supported by the European Network of Excellence on Complex Metallic Alloys CMA under contracts No. NMP3-CT-2005-500145 and by the Agence Nationale de la Recherche, reference ANR-07-Blan-0270. Work at the Ames Laboratory was supported by the Department of Energy – Basic Energy Sciences under Contract No. DE- AC02-07CH11358.

References

[1] R. Dariola, J.J. Lewandowski, C.T. Liu, P.L. Martin, D.B. Miracle, M.V. Nathal, Structural Intermetallics, The Minerals, Metals & Materials Society, Warrendale, PA, 1993.
[2] D.B. Miracle, Overview No. 104 The physical and mechanical properties of NiAl, Acta Metallurgica et Materialia 41 (1993) 649–684.
[3] B.D. Cullity, C.D. Graham, Introduction to Magnetic Materials, Wiley and IEEE Press, Hoboken, New Jersey, 2009.
[4] K. Oikawa, L. Wulff, T. Iijima, F. Gejima, T. Ohmori, A. Fujita, K. Fukamichi, R. Kainuma, K. Ishida, Promising ferromagnetic Ni–Co–Al shape memory alloy system, Applied Physics Letters 79 (2001) 3290–3292.
[5] J.M. Dubois, Useful Quasicrystals, World Scientific, Singapore, 2005.
[6] V. Blum, L. Hammer, C. Schmidt, W. Meier, O. Wieckhorst, S. Müller, K. Heinz, Segregation in strongly ordering compounds: a key role of constitutional defects, Physical Review Letters 89 (2002) 266102.
[7] L. Hammer, W. Meier, V. Blum, K. Heinz, Equilibration processes in surfaces of the binary alloy Fe–Al, Journal of Physical Chemistry 14 (2002) 4145–4164.
[8] L. Hammer, H. Graupner, V. Blum, K. Heinz, G.W. Ownby, D.M. Zehner, Segregation phenomena on surfaces of the ordered bimetallic alloy FeAl, Surface Science 412 (413) (1998) 69–81.
[9] M. Yamasaki, A.P. Tsai, Oxidation behavior of quasicrystalline $Al_{63}Cu_{25}Fe_{12}$ alloys with additional elements, Journal of Alloys and Compounds 342 (2002) 473–476.
[10] M. Kottcke, H. Graupner, D.M. Zehner, L. Hammer, K. Heinz, Segregation-induced subsurface restructuring of FeAl(100), Physical Review B 54 (1996) R5275–R5278.
[11] D.R. Mullins, S.H. Overbury, The structure and composition of the NiAl(110) and NiAl(100) surfaces, Surface Science 199 (1988) 141–153.
[12] R. Franchy, J. Masuch, P. Gassmann, The oxidation of the NiAl(111) surface, Applied Surface Science 93 (1996) 317–327.
[13] X. Torrelles, F. Wendler, O. Bikondoa, H. Isern, W. Moritz, G.R. Castro, Structure of the clean NiAl(110) surface and the Al2O3/NiAl(110) interface by measurements of crystal truncation rods, Surface Science 487 (2001) 97–106.
[14] S.M. Yalisove, W.R. Graham, Multilayer rippled structure of the Nil(110) service. A medium energy ion scattering study, Surface Science 183 (1987) 556–564.
[15] M.H. Kang, E.J. Mele, NiAl(110) surface. First-principles determination of the rippled relaxation, Physical Review B 36 (1987) 7371–7377.
[16] H.L. Davis, J.R. Noonan, Rippled relaxation in the (110) surface of the ordered metallic alloy NiAl, Physical Review Letters 54 (1985) 566–569.
[17] S.-C. Lui, M.H. Kang, E.J. Mele, E.W. Plummer, Surface states on NiAl(110), Physical Review B 39 (1989) 13149–13159.
[18] W. Song, M. Yoshitake, X-ray photoelectron spectroscopy and low-energy electron diffraction study on the oxidation of NiAl(110) surfaces at elevated temperatures, Thin Solid Films 464–465 (2004) 52–56.

[19] R. McGrath, J.A. Smerdon, H.R. Sharma, W. Theis, J. Ledieu, The surface science of quasicrystals, Journal of Physics: Condensed Matter 22 (2009) 084022.
[20] V. Fournée, J. Ledieu, P. Thiel (Eds.), Cluster issue: ''quasicrystals at interfaces'', Journal of Physics: Condensed Matter, 20 (2008) 310301–315208.
[21] H.R. Sharma, M. Shimoda, A.P. Tsai, Quasicrystal surfaces: structure and growth of atomic overlayers, Advances in Physics 56 (2007) 403–464.
[22] T. Duguet, E. Gaudry, T. Deniozou, J. Ledieu, M.C. de Weerd, T. Belmonte, J.M. Dubois, V. Fournée, Complex metallic surface phases in the Al/Cu(111) system: An experimental and computational study, Physical Review B 80 (2009) 205412.
[23] T. Duguet, J. Ledieu, J.M. Dubois, V. Fournée, Surface alloys as interfacial layers between quasicrystalline and periodic materials, cluster issue on ''Quasicrystals at Interfaces'', Journal of Physics: Condensed Matter 20 (2008) 314009.
[24] T. Duguet, S. Kenzari, V. Demange, T. Belmonte, J.-M. Dubois, V. Fournée, Structurally complex metallic coatings in the Al–Cu system and their orientation relationships with an icosahedral quasicrystal, Journal of Materials Research 25 (2010) 764–772.
[25] Y. Sugimoto, P. Pou, M. Abe, P. Jelinek, R. Perez, S. Morita, O. Custance, Chemical identification of individual surface atoms by atomic force microscopy, Nature 446 (2007) 64–67.
[26] C. Weiss, C. Wagner, C. Kleimann, F.S. Tautz, R. Temirov, Resolving chemical structures in scanning tunnelling microscopy, [cond-mat.mes-hall], (2009).
[27] C.J. Chen, A universal relation in NC-AFM, STM, and atom manipulation, Nanotechnology 16 (2005) S27.
[28] J.E. Frommer, Imaging chemical bonds by SPM, NATO ASI Series E 286 (1995) 551–566.
[29] R.J. Hamers, Scanned probe microscopies in chemistry, The Journal of Physical Chemistry 100 (1996) 13103–13120.
[30] Y. Manassen, S. Dov, Scanning Tunneling Microscopy (STM) on Physisorbed Chemical Groups of Individual Immobilized Molecules, Annals of the New York Academy of Sciences 852 (1998) 277.
[31] D.L. Patrick, T.P. Beebe, Scanning tunneling and atomic force microscopy: Tools for imaging the chemical state, in: M.D. Morris (Ed.), Microscopic and Spectroscopic Imaging of the Chemical State, CRC Press, Boca Raton, FL, 1993, p. 159.
[32] T.T. Tsong, Toward single atom chemical analysis with STM, e-Journal of Surface Science and Nanotechnology 1 (2003) 102–105.
[33] M. Ternes, M. Pivetta, F. Patthey, W.-D. Schneider, Creation, electronic properties, disorder, and melting of two-dimensional surface-state-mediated adatom superlattices, Progress in Surface Science 85 (2010) 1–27.
[34] M.F. Crommie, C.P. Lutz, D.M. Eigler, Confinement of electrons to quantum corrals on a metal surface, Science 262 (1993) 218–220.
[35] L. Jurczyszyn, A. Rosenhahn, J. Schneider, C. Becker, K. Wandelt, Formation of STM images of Ni_3Al (001) and (111) surfaces, Physical Review B 68 (2003) 115425.
[36] J. Li, W.-D. Schneider, R. Berndt, Local density of states from spectroscopic scanning-tunneling-microscope images: Ag(111), Physical Review B 56 (1997) 7656.
[37] J. Wintterlin, J. Wiechers, H. Brune, T. Gritsch, H. Hofer, R.J. Behm, Atomic-resolution imaging of close-packed metal surfaces by scanning tunneling microscopy, Physical Review Letters 62 (1989) 59.
[38] E. Belin-Ferré (Ed.), Basics of thermodynamics and phase transitions in complex intermetallics, World Scientific, Singapore, 2008.
[39] J. Tersoff, D.R. Hamann, Theory of the scanning tunneling microscope, Physical Review B 31 (1985) 805.
[40] J. Bardeen, Tunnelling from a many-particle point of view, Physical Review Letters 6 (1961) 57–59.
[41] T. Duguet, B. Unal, M.C.d. Weerd, J. Ledieu, R.A. Ribeiro, P.C. Canfield, S. Deloudi, W. Steurer, C.J. Jenks, J.M. Dubois, V. Fournee, P.A. Thiel, Twofold surface of the decagonal Al–Cu–Co quasicrystal, Physical Review B 80 (2009) 024201.
[42] S. Deloudi, Ph.D. Thesis, Eidgenössische Technische Hochschule thesis No. 18107, Zurich, 2008.
[43] W. Steurer, K.H. Kuo, Five-dimensional structure analysis of decagonal $Al_{65}Cu_{20}Co_{15}$, Acta Crystallographica B 46 (1990) 703–712.
[44] M. Krajci, J. Hafner, M. Mihalkovic, Electronic structure and transport properties of decagonal Al–Cu–Co alloys, Physical Review B 56 (1997) 3072.
[45] J.Y. Park, D.F. Ogletree, M. Salmeron, R.A. Ribeiro, P.C. Canfield, C.J. Jenks, P.A. Thiel, Atomic scale coexistence of periodic and quasiperiodic order in a 2-fold Al–Ni–Co decagonal quasicrystal surface, Physical Review B 72 (2005) 220201.
[46] R. Mäder, R. Widmer, P. Gröning, P. Ruffieux, W. Steurer, O. Gröning, A comparative scanning tunneling spectroscopy investigation of the (12110)-surface of decagonal Al–Ni–Co and the (100)-surface of its approximant Y–Al–Ni–Co, New Journal of Physics 12 (2010) 073043.
[47] R. Mäder, R. Widmer, P. Gröning, S. Deloudi, W. Steurer, M. Heggen, P. Schall, M. Feuerbacher, O. Gröning, High-resolution scanning tunneling microscopy investigation of the (12110) and (10000) two-fold symmetric d-Al–Ni–Co quasicrystalline surfaces, Physical Review B 80 (2009) 035433.
[48] N. Ferralis, K. Pussi, E.J. Cox, M. Gierer, J. Ledieu, I.R. Fisher, C.J. Jenks, M. Lindroos, R. McGrath, R.D. Diehl, Structure of the tenfold d-Al–Ni–Co quasicrystal surface, Physical Review B 69 (2004) 153404.
[49] J. Yuhara, J. Klikovits, M. Schmid, P. Varga, Y. Yokoyama, T. Shishido, K. Soda, Atomic structure of an Al–Co–Ni decagonal quasicrystalline surface, Physical Review B 70 (2004) 024203.
[50] S. Balanetskyy, G. Meisterernst, M. Heggen, M. Feuerbacher, Reinvestigation of the Al–Mn–Pd alloy system in the vicinity of the T- and R-phases, Intermetallics 16 (2008) 71–87.
[51] M. Taylor, The space group of $MnAl_3$, Acta Crystallographica 14 (1961) 84.
[52] V. Simonet, F. Hippert, M. Audier, G. Trambly de Laissardière, Origin of magnetism in crystalline and quasicrystalline AlMn and AlPdMn phases, Physical Review B 58 (1998) R8865–R8868.
[53] V. Simonet, F. Hippert, M. Audier, Y. Calvayrac, Magnetism of approximants in the Al–Mn and Al–Pd–Mn systems, Materials Science and Engineering A 294–296 (2000) 625–628.
[54] F. Hippert, V. Simonet, G.T.d. Laissardière, M. Audier, Y. Calvayrac, Magnetic properties of AlPdMn approximant phases, Journal of Physics: Condensed Matter 11 (1999) 10419.
[55] J. Hafner, M. Krajčí, Formation of magnetic moments in crystalline, quasicrystalline, and liquid Al–Mn alloys, Physical Review B 57 (1998) 2849–2860.

[56] M. Heggen, M. Feuerbacher, Metadislocation arrangements in the complex metallic alloy ξ′-Al–Pd–Mn, Philosophical Magazine 86 (2006) 985–990.
[57] T. Deniozou, R. Addou, A.K. Shukla, M. Heggen, M. Feuerbacher, M. Krajci, J. Hafner, R. Widmer, O. Groning, V. Fournee, J.-M. Dubois, J. Ledieu, Structure of the (010) surface of the orthorhombic complex metallic alloy T-Al3(Mn, Pd), Physical Review B 81 (2010) 125418.
[58] B. Unal, C.J. Jenks, P.A. Thiel, Comparison between experimental surface data and bulk structure models for quasicrystalline AlPdMn: average atomic densities and chemical compositions, Physical Review B 77 (2008) 195419.
[59] M. Krajci, J. Hafner, J. Ledieu, R. McGrath, Surface vacancies at the fivefold icosahedral Al–Pd–Mn quasicrystal surface: a comparison of ab initio calculated and experimental STM images, Physical Review B 73 (2006) 024202.
[60] E. Belin, Z. Dankhazi, A. Sadoc, J.M. Dubois, Electronic distributions in quasicrystalline Al–Pd–Mn alloys, Journal of Physics: Condensed Matter 6 (1994) 8771.
[61] R. Addou, E. Gaudry, T. Deniozou, M. Heggen, M. Feuerbacher, P. Gille, Y. Grin, R. Widmer, O. Groening, V. Fournee, J.-M. Dubois, J. Ledieu, Structure investigation of the (100) surface of the orthorhombic $Al_{13}Co_4$ crystal, Physical Review B 80 (2009) 014203.
[62] H. Shin, K. Pussi, É. Gaudry, J. Ledieu, V. Fournée, S. Alarcón Villaseca, J.M. Dubois, Y. Grin, P. Gille, W. Moritz, R.D. Diehl, Structure of the orthorhombic $Al_{13}Co_4$(100) surface using LEED, STM, and ab initio studies, Physical Review B 84 (2011) 085411.
[63] M. Krajčí, J. Hafner, Surface structures of complex intermetallic compounds: an ab initio DFT study for the (100) surface of o-$Al_{13}Co_4$, Physical Review B 84 (2011) 115410.
[64] S.A.n. Villaseca, J. Ledieu, L.N. Serkovic Loli, M.C. de Weerd, P. Gille, V. Fournée, J.M. Dubois, E. Gaudry, Structural investigation of the (0 0 1) surface of the Al9Co2 complex metallic alloy, The Journal of Physical Chemistry C 115 (2011) 14922–14932.
[65] H.L. Davis, J.R. Noonan, Rippled relaxation in the (110) surface of the ordered metallic alloy NiAl, Physical Review Letters 54 (1985) 566.
[66] K. Ojrup Hansen, J. Gottschalck, L. Petersen, B. Hammer, E. Laegsgaard, F. Besenbacher, I. Stensgaard, Surface waves on NiAl(110), Physical Review B 63 (2001) 115421.
[67] L. Jurczyszyn, A. Krupski, S. Degen, B. Pieczyrak, M. Kralj, C. Becker, K. Wandelt, Atomic structure and electronic properties of Ni_3Al(111) and (011) surfaces, Physical Review B 76 (2007) 0445101.
[68] L. Piccolo, L. Barbier, Chemical order driven morphology of a vicinal surface of Fe_3Al(1 1 1): an He diffraction and STM study, Surface Science 505 (2002) 271–284.
[69] M. Bielmann, A. Barranco, P. Ruffieux, O. Gröning, R. Fasel, R. Widmer, P. Gröning, Formation of Al_4Cu_9 on the 5 fold surface of icosahedral AlPdMn, Advanced Engineering Materials 7 (2005) 392.
[70] E. Gaudry, A.K. Shukla, T. Duguet, J. Ledieu, M.-C. de Weerd, J.-M. Dubois, V. Fournee, Structural investigation of the (110) surface of gamma-Al4Cu9, Physical Review B 82 (2010) 085411.
[71] M. Hoheisel, J. Kuntze, S. Speller, A. Postnikov, W. Heiland, I. Spolveri, U. Bardi, Metastable and equilibrium structures on Pt_3Sn(001) studied by STM, RHEED, LEED, and AES, Physical Review B 60 (1999) 2033–2039.
[72] U. Mizutani, A. Kamiya, Electronic specific heat measurements for quasicrystals and Frank–Kasper crystals in Mg–Al–Ag, Mg–Al–Cu, Mg–Al–Zn, Mg–Ga–Zn and Al–Li–Cu alloy systems, Journal of Physics: Condensed Matter 3 (1991) 3711.
[73] M. Schmid, P. Varga, Chapter 4 segregation and surface chemical ordering – an experimental view on the atomic scale, in: D.P. Woodruff (Ed.), The Chemical Physics of Solid Surfaces, Elsevier, New York, 2002, pp. 118–151.
[74] M. Schmid, H. Stadler, P. Varga, Direct observation of surface chemical order by scanning tunneling microscopy, Physical Review Letters 70 (1993) 1441–1444.
[75] E.L.D. Hebenstreit, W. Hebenstreit, M. Schmid, P. Varga, $Pt_{25}Rh_{75}$(111), (110), and (100) studied by scanning tunnelling microscopy with chemical contrast, Surface Science 441 (1999) 441–453.
[76] Y. Gauthier, P. Dolle, R. Baudoing-Savois, W. Hebenstreit, E. Platzgummer, M. Schmid, P. Varga, Chemical ordering and reconstruction of $Pt_{25}Co_{75}$(100): an LEED/STM study, Surface Science 396 (1998) 137–155.
[77] Y.-F. Wang, W.-B. Zhang, Z.-Z. Wang, Y.-H. Deng, N. Yu, B.-Y. Tang, X.-Q. Zeng, W.-J. Ding, First-principles study of structural stabilities and electronic characteristics of Mg–La intermetallic compounds, Computational Materials Science 41 (2007) 78–85.
[78] S. Tuncel, R.-D. Hoffmann, B. Chevalier, S.F. Matar, R. Pöttgen, Cobalt Centered Trigonal RE6 Prisms and Mg_4 Clusters as Basic Structural Units in RE_4CoMg (RE = Y, La, Pr, Nd, Sm, Gd–Tm), Zeitschrift für anorganische und allgemeine Chemie 633 (2007) 151–157.